Supporting Information

Cytoplasmic Viscosity is a Potential Biomarker for Metastatic Breast Cancer Cells

Marie Dessard[1,2] Jean-Baptiste Manneville[1] and Jean-François Berret[1]*
[1]Université Paris Cité, CNRS, Matière et systèmes complexes, 75013 Paris, France
[2]CNRS, INSERM, CIML, Luminy Campus, Aix-Marseille University, 13009 Marseille, France

Outline

Additional supporting information

Original avi-file: "Movie#1A of a 3µm wire in MCF10A at 0.02 rad s-1_cell scale.avi"
Movie of a 3 µm magnetic wire undergoing a synchronous motion at the angular frequency of 0.02 rad s^{-1} and under a magnetic field of 12 mT. Total movie time is 564 s.
Original avi-file: "Movie#1B of a 3µm wire in MCF10A at 0.02 rad s-1_NW scale.avi"
Same as Movie#1A with close-up view around the magnetic wire.

Original avi-file: "Movie#2A of a 3µm wire in MCF10A at 0.44 rad s-1_cell scale.avi"
Movie of a 3 µm magnetic wire undergoing intermittent phases of rotation and oscillation at the angular frequency of 0.44 rad s^{-1} and under a magnetic field of 12 mT. Total movie time is 60 s.
Original avi-file: "Movie#2B of a 3µm wire in MCF10A at 0.44 rad s-1_NW scale.avi"
Same as Movie#2A with close-up view around the magnetic wire.

Original avi-file: "Movie#3A of a 3µm wire in MCF10A at 9.4 rad s-1_cell scale.avi"
Movie of a 3 µm magnetic wire undergoing asynchronous oscillations at the angular frequency of 9.4 rad s^{-1} and under a magnetic field of 12 mT. Total movie time is 9.0 s.
Original avi-file: "Movie#3B of a 3µm wire in MCF10A at 9.4 rad s-1_NW scale.avi"
Same as Movie#3A with close-up view around the magnetic wire.

Original avi-files:
"Movie4 - NW Internalization in NIH/3T3 cell.avi",

“Movie5 - NW Internalization in NIH/3T3 cell.avi” and
Movies showing different internalization process of magnetic wires into NIH/3T3 murine fibroblasts.

Excel- file – “Microrheology data on MCF-10A, MCF-7 and MDA-MB-231”
This file contains all data relating to measurements made on the three cell lines MCF-10A, MCF-7, and MDA-MB-231 cells. In addition to the geometrical characteristics of the nanowires studied (length, diameter), values for ω_C, θ_B-values at ω/ω_C = 1000 and L^* are provided. Static viscosity η and elastic modulus G values are also given.

Keywords: Cell mechanics - Microrheology - Breast cancer cells – Viscoelasticity - Metastatic Potential – Magnetic Rotational Spectroscopy

Corresponding authors: jean-francois.berret@u-paris.fr
Revised version submitted to Nanoscale Advances
Wednesday, February 7, 2024

Supporting Information S1

Calibration of the sonicated wire magnetic properties and determination of the cytoplasm viscosity

The calibration of the wire magnetic properties was performed on an aqueous glycerol solution of weight (resp. volume) fraction of c = 93.6 wt. % (resp. φ = 92.0 vol. %) at 32.5 °C. At this temperature, the viscosity is η_{WG} = 0.159 Pa s [1]. For the calibration, we have strictly complied with the same experimental conditions as for the cell measurements: same γ-Fe_2O_3@PAA_{2k}-PDADMAC wires, same magnetic field (B = 12 mT) and same positions of the wires in the measurement chamber, especially regarding their distance to the magnetic coils. In this way we minimize the errors attributable to the environment of the measuring chamber. The other advantage is, as we will see, that it allows us to obtain the cytoplasm viscosity values in a simpler way.

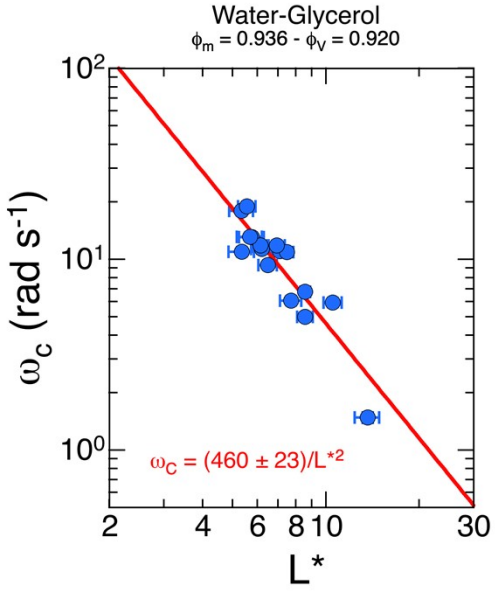

Figure S1 : *Critical frequency as a function of the reduced wire length obtained from a c = 0.936 wt. % aqueous glycerol solution. The straight line indicates the best fit using a non-linear least squares analysis with Eq. S1-1*

Fig. S1 displays the critical frequency ω_C as a function of the reduced length L* for wires dispersed in a c = 93.6 wt. % aqueous glycerol solution. The data is then adjusted with the expression:

$$\omega_C = \frac{3\ \Delta\chi\ B^2}{8\mu_0\eta_{WG}L^{*2}} \qquad (S1-1),$$

leading to the prefactor in front of the $1/L^{*2}$-dependence:

$$\frac{3\ \Delta\chi}{8\mu_0\eta_{WG}}B^2 = 460\ \pm\ 23\ rad\ s^{-1} \qquad (S1-2)$$

From Eq. S1-2, we obtain for the anisotropy of susceptibility between parallel and perpendicular directions $\Delta\chi = \chi^2/(2+\chi)$ = 1.71 ± 0.09.

We can also express the viscosity of any fluid measured under the experimental conditions used, including that of MCF-10A, MCF-7 and MDA-MB-231 cells, as:

$$\eta_{Cell} = \frac{73.28}{\omega_C(L^*)L^{*2}} \qquad (S1-3)$$

where the coefficient 73.28 is the product of the viscosity of the calibration fluid (0.159 Pa s) and the factor 460 rad s^{-1}. It is thus understood that the viscosity for living cells is accessible from the knowledge of the critical frequency $\omega_C(L^*)$ and the reduced length L^*. The data corresponding to the three cell lines shown in **Figs. 2 and 3** in the main text.

Supporting Information S2

Evidence of the $\omega_C \sim 1/L^{*2}$ regime in a viscous fluid and in a viscoelastic fluid

In this section, we employ the MRS technique to investigate the behavior of magnetic wires integrated within living cells, focusing on two widely studied model fluids: an aqueous glycerol solution and a surfactant solution representing a Maxwell fluid.

A – MRS in a purely viscous fluid

Magnetic rotational spectroscopy experiments were performed on a c = 95.96 wt. % aqueous glycerol solution using γ-Fe_2O_3@PAA_{2k}-PDADMAC magnetic wires between 4 to 68 µm. At the temperature of the experiment (T = 32 °C), the fluid viscosity was 0.247 Pa s [1]. The experiments were performed at 5 different values of the magnetic fields, 2.27, 4.54, 9.07, 13.6 mT and 17.01 mT, resulting in a total of 177 wires studied.

The data in **Fig. S2-A** shows the reduced critical frequency $8\mu_0\omega_C\eta/3\Delta\chi B^2$ as a function of L^*. The straight line between the data corresponds to the law $8\mu_0\omega_C\eta/3\Delta\chi B^2 = 1/L^{*2}$, in good agreement with the model (Eq. 1, main text).

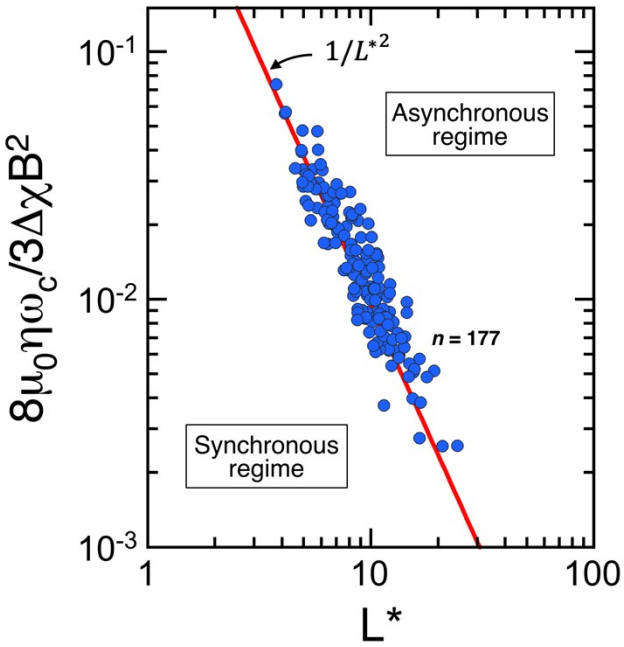

Figure S2-A: *Critical frequency* $8\mu_0\omega_C\eta/3\Delta\chi B^2$ *as a function of the parameter* $L^* = L/[D\sqrt{g(L/D)}]$ *obtained for wires dispersed in an aqueous glycerol solution of static viscosity* η *= 0.247 Pa s. The straight line is calculated using the model developed in Ref.[2,3].*

B – MRS in a model Maxwell viscoelastic fluid

The solution studied is a mixture of cetylpyridinium chloride (CPCl) and sodium salicylate (NaSal) in 0.5 M NaCl brine at c = 12%. CPCl/NaSal are known to self-assemble spontaneously into micrometer-length wormlike micelles and to build an entangled network in the semi-dilute regime. This network imparts a Maxwell-type viscoelastic behavior to the solution [4-7].

Fig. S2-B shows the normalized elastic and loss moduli, respectively $G'(\omega)/G_0$ and $G''(\omega)/G_0$ as a function of normalized frequency, $\omega\tau$ at different temperatures, T = 20 °C, 30 °C and 40 °C. The data are superimposed and well accounted for by the Maxwell model predictions (continuous curve in gray) [4].

Subsequently, the CPCl/NaSal surfactant solution was diluted to a concentration of 7.72 wt.% and subjected to magnetic rotational spectroscopy under the same conditions as the living cells studied. At body temperature (T = 37 °C), the surfactant solution retains its Maxwell-type viscoelastic character, with an estimated viscosity of η = 5.5 Pa s, an instantaneous elastic modulus G = 110 Pa and a relaxation time of τ = 0.05 s [4]. Note that here, viscosity and modulus of elasticity are close to those of living cells, and their overall behavior can be paralleled to that of cells, with both systems exhibiting viscoelastic properties. In **Fig. S2-C**, the behavior of $\omega_C(L^*)$ for surfactant micelles is depicted. Specifically, the anticipated relationship $\omega_C(L^*) \sim 1/L^{*2}$ is observed and effectively modeled for the wormlike micelles. The viscosity value obtained from the $1/L^{*2}$ dependence also agrees with the estimated wormlike micelle viscosity. Moreover, within the L^* range of 2-12, the critical frequency varies by a factor of around 30, whereas for the living cells, this factor is 1000 (**Fig. 2**, main text), indicating for the later a much stronger L^*-dependence.

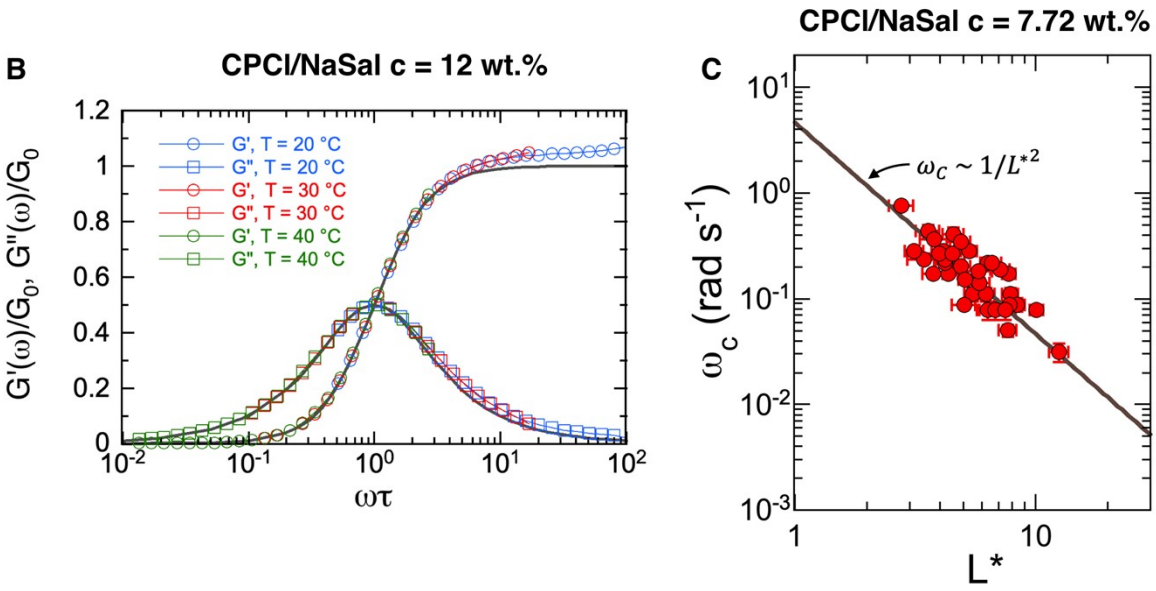

Figure S2-B: *Normalized elastic and loss moduli of CPCl/NaSal wormlike micelles at c = 12 wt. %, together with the fitting of the Maxwell model (gray continuous lines)*

Figure S2-C: *Variation of the critical frequency ω_C as a function of the reduced wire length $L^* = L/[D\sqrt{g(L/D)}]$ for CPCl/NaSal wormlike micellar solution at c = 7.72 wt. %. The straight line is the power law with exponent -2.*

Supporting Information S3

Complementary Scanning electron microscopy and EDX data

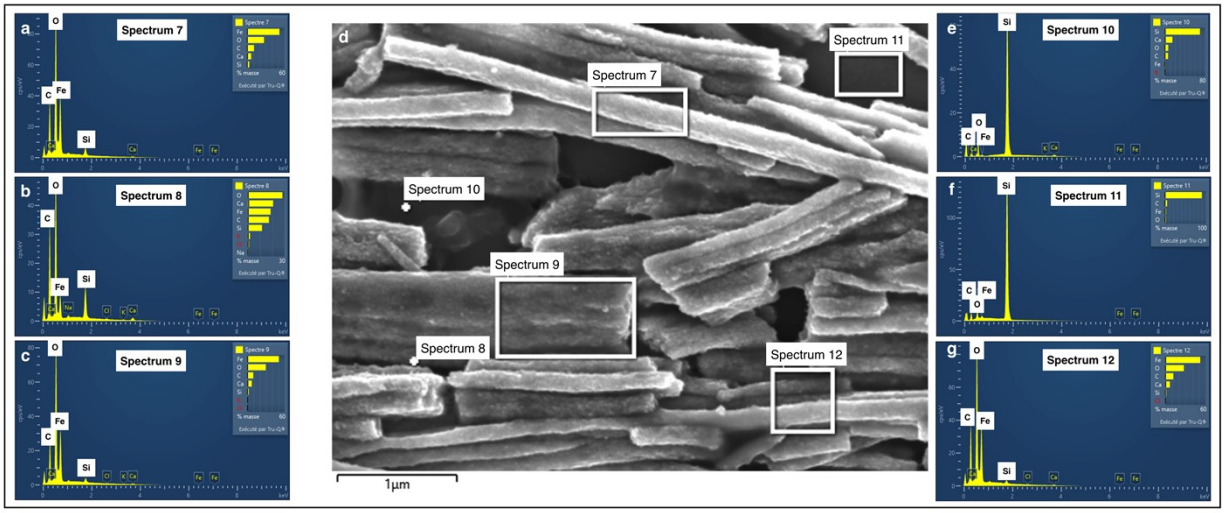

Figure S3 : *Scanning electron microscopy of sonicated magnetic wires and associated EDX elemental proportions of iron, oxygen, carbon and silicon (spectra 7 to 12). The rectangles shown in the central figure denote the area to which the EDX technique has been applied.*

Supporting Information S4

Sampling wires according to their length and effect on the viscosity

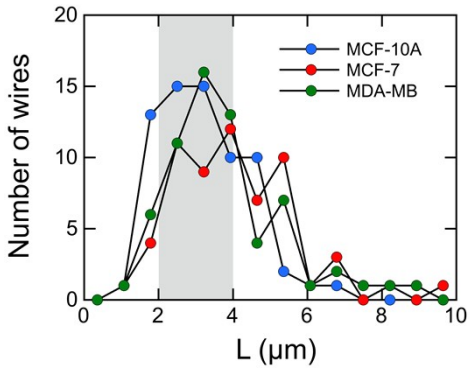

***Figure S4-A**: Length distribution of wires used in MRS experiments on MCF-10A, MCF-7, and MDA-MB-231 cells. Wires with sizes between 2 and 4 μm (shaded area) represent 50-60% of the total number. The viscosity values of MCF-10A, MCF-7, and MDA-MB-231 cells provided in Table I (main text) are those obtained in the interval 2-4 μm.*

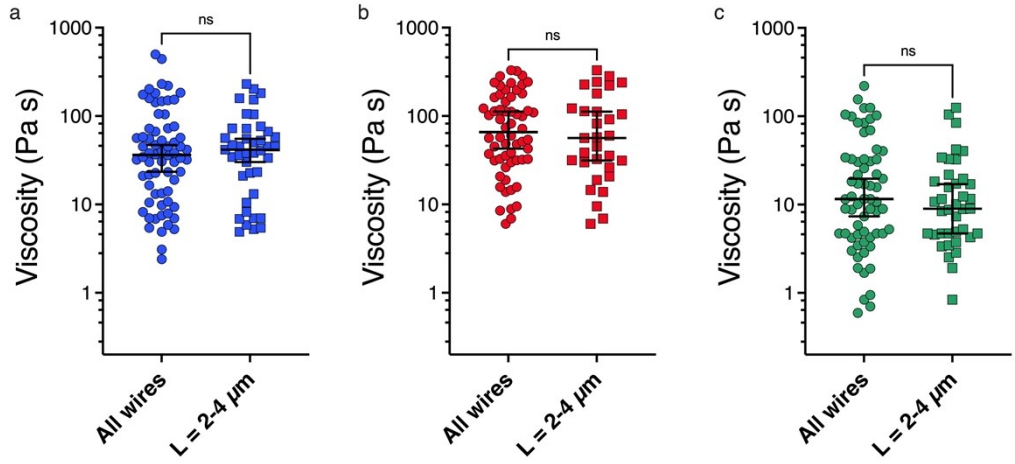

***Figure S4-B :** Static viscosity for a) MCF-10A, b) MCF-7, and c) MDA-MB-231 for all wires (circles) and for wires with lengths between 2 μm and 4 μm (squares). The median value with 95% confidence interval, and standard errors are shown. The corresponding values are shown in **Table S4**.*

Cells	Wire length	Data points	Median viscosity (Pa s)	Std. error (Pa s)
MCF-10	All L	68	36.3	11.2
	L = 2-4 μm	41	41.6	8.7
MCF-7	All L	60	65.9	11.4
	L = 2-4 μm	31	56.4	16.6
MDA-MB-231	All L	68	12.0	5.7
	L = 2-4 μm	43	10.7	5.4

***Table S1 :** Comparison between median viscosities obtained for all wires tested and for wires with lengths between 2 and 4 μm.*

Supporting Information S5

$\omega_C(L^*)$ versus L data for NIH/3T3 mouse fibroblasts and HeLa cervical cancer cells, with new adjustments

We recall here the results obtained with the MRS technique on NIH/3T3 mouse fibroblasts and HeLa cervical cancer cells [8,9]. **Figs. S5a and S5b** display the dependences of the critical frequency ω_C as a function of the reduced wire length L^*. Least square calculations using a power law dependence of the form $\omega_C(L^*) \sim 1/L^{*\alpha}$ provide exponents α = 3.5 ± 0.5 and α = 6.5 ± 0.5 for NIH/3T3 and HeLa, respectively. The intracellular viscosity was computed from ω_C and L^*-values for each of the 29 internalized wires. **Fig. S5c** shows a scatter dotplot of the viscosity of NIH/3T3 and HeLa cells for the n = 19 and n = 10. Median viscosities were found at $\eta_{NIH/3T3}$ = 47.4 ± 7.2 Pa s, η_{HeLa} = 21.4 ± 16.0 Pa s (**Fig. S5d**). Statistical significance using Student's t-test for unpaired samples was found to be non-significant between the two cell lines. These results point to the need to conduct experiments on a large scale to enhance the reliability and validity of conclusions drawn about intracellular viscosity. They also show that the deviation from the model prediction had already been achieved in the first microrheology assays. The interpretation of the data in Ref. [8] proposed here is new and different from what had previously been made.

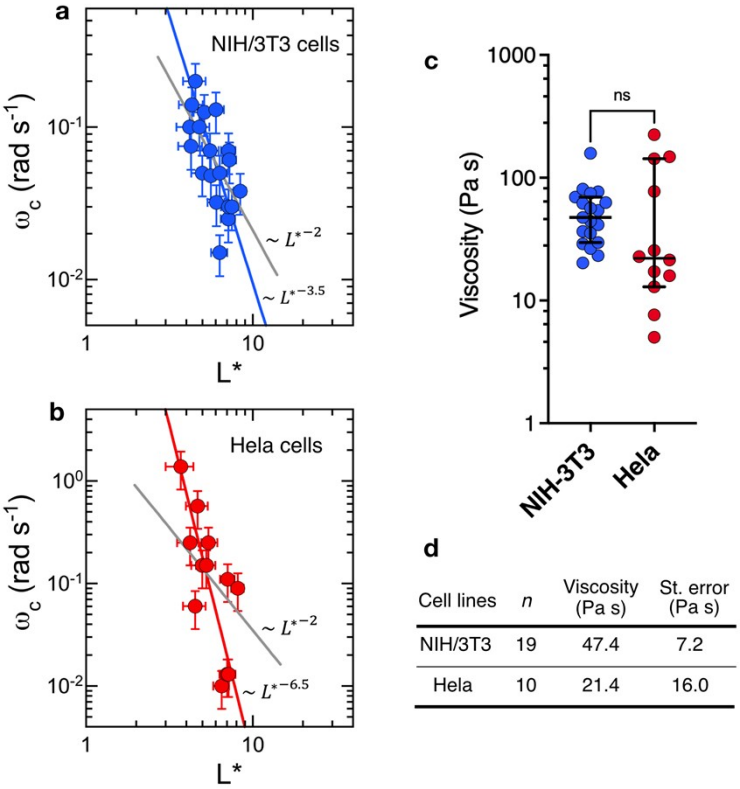

Cell lines	*n*	Viscosity (Pa s)	St. error (Pa s)
NIH/3T3	19	47.4	7.2
Hela	10	21.4	16.0

Figure S5 : *Variation of the critical frequency ω_C as a function of the reduced wire length $L^* = L/[D\sqrt{g(L/D)}]$ for* ***a)*** *NIH/3T3 mouse fibroblasts, and* ***b)*** *HeLa cervical cancer cells. The straight lines with the same color as the data are power laws of exponent -3.5 and -6.5, respectively. Straight lines in gray are from Eq. 1 (main text).* ***c)*** *Static viscosity boxplots for NIH/3T3 fibroblasts and HeLa cervical cancer cells.* ***d)*** *Table summarizing the viscosity data for these cell lines.*

Supporting Information S6

Analytical derivation of the critical frequency exponent in cells

We here derive the scaling law exponent of viscosity as a function of wire length analytically. To do that, we first recall the expression of the critical frequency ω_C:

$$\omega_C = \frac{3}{8\mu_0\eta(L)} \Delta\chi\, g\left(\frac{L}{D}\right)\frac{D^2}{L^2}B^2 = \frac{3}{8\mu_0\eta(L)} \frac{\Delta\chi\ B^2}{L^{*2}} \qquad (S6-1)$$

where $L^* = L/[D\sqrt{g(L/D)}]$. In the previous equation, we assume that the viscosity of the cytoplasm depends on the wire length, and we hypothesize a variation of the form $\eta(L) \sim L^{\alpha}$. In the following, we show that the power law agrees with the experimental data and determine the exponent α.

Fig. S6-A displays the L-dependence of the diameter $D(L)$, of the function $g(L/D)$ and of the reduced length $L^*(L)$.

The observed slight variation in diameter with the length of the wire, characterized by a scaling exponent between 0.20 and 0.25, is a consequence attributed to the specific wire synthesis method employed (**Fig. S6-Aa, S6-Ad and S6-Ag**). Such a result has already been discussed in a recent work [10].

The function $g(L/D)$ was derived by Tirrado et al. [11] and is valid for aspect ratios between L/D = 2 and 20, which is the case in our study. In the region of interest, *i.e.* for L = 2-4 µm (which represents the interval where we have 50-60% of the wires), $g(L/D)$ is an increasing function that varies as $L^{0.6}$ (**Fig. S6-Ab, S6-Ae and S6-Ah**).

Combining the two previous variations, this gives for L^*:

$$L^*(L) \sim L^{\beta} \qquad (S6-2)$$

with $\beta \sim 1/2$

For the three cell lines, **Fig. S6-Ac, Af and Ai** give exponents β of 0.441, 0.446 and 0.494 respectively.

By replacing this expression in Eq. S6-1 and taking into account the power law for viscosity $\eta(L) \sim L^{\alpha}$, the critical frequency reads :

$$\omega_C = \frac{3}{8\mu_0\eta_0} \frac{\Delta\chi\ B^2}{L^{*\left(2+\frac{\alpha}{\beta}\right)}} \qquad (S6-3)$$

The results in **Fig. 2** (main text) show that $2+\frac{\alpha}{\beta}$ = 7, leading to $\alpha = 5\beta$. With the values found for β, we obtain $\alpha_{MCF-10A}$ = 2.2, α_{MCF-7} = 2.3, and $\alpha_{MDA-MB-231}$ = 2.5.

The previous rationale shows that a moderate dependence of the cytoplasm viscosity with wire length produces a significant variation in the critical frequency ω_C. Of note, this result does not seem to be related to the invasive and metastatic potential of the cells studied.

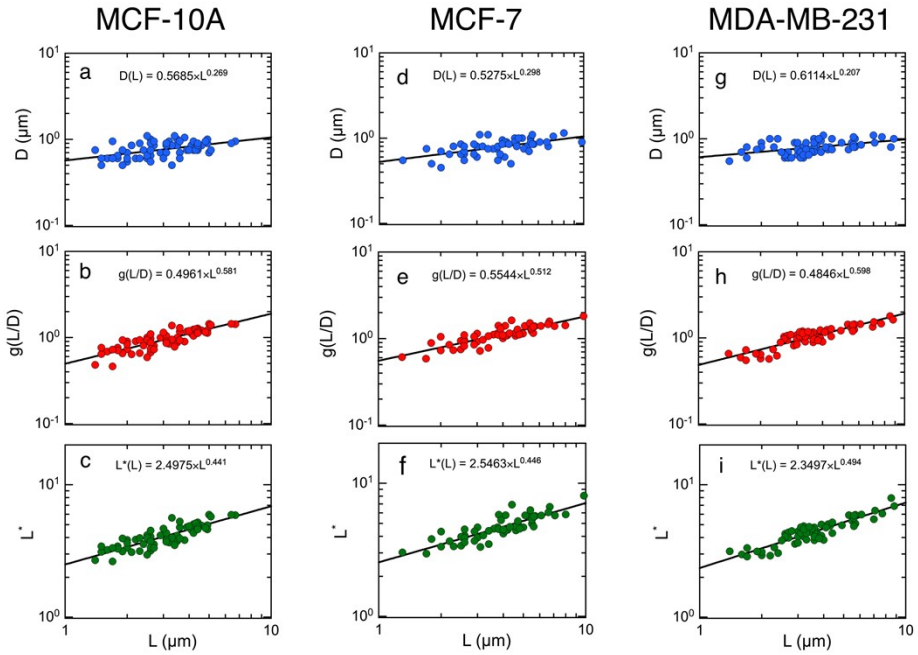

Figure S6-A : *L-dependences of the diameter D, of the function g(L/D) and of the reduced length* L^* *found from the experimental data collected in this study.*

Fig. S6-B displays the L-dependence of the viscosity by organizing the data into 6 subgroups of equal size and taking the median value. This representation allows us to obtain directly the exponents of the $\eta(L) \sim L^{\alpha}$ law. The exponents are in fair agreement with those determined previously, showing a near-to-quadratic length dependency.

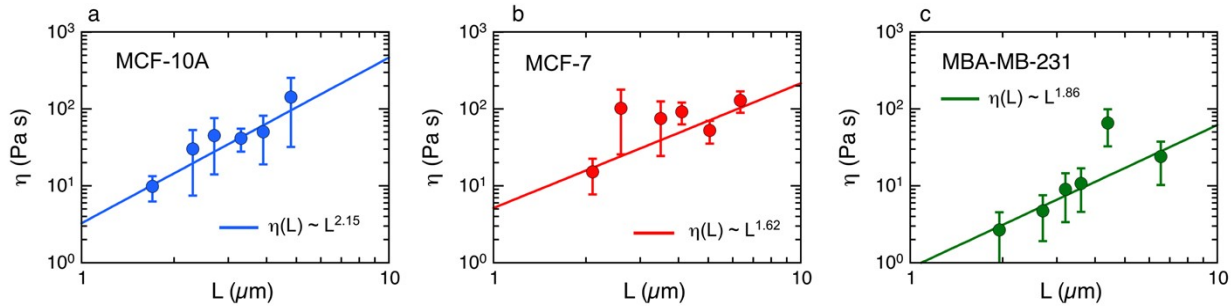

Figure S6-B : *Variation of the viscosity as a function of the wire length L obtained from MRS experiments for* ***a)*** *MCF-10A,* ***b)*** *MCF-7 and* ***c)*** *MDA-MB-231 respectively. The straight lines in the figures result from best fit calculations using a scaling with exponents 2.15, 1.62 and 1.86.*

Supporting Information S7

Evolution of the intracellular viscosity and elastic modulus as a function of the number of wires investigated

We recall here that the intracellular viscosity and elastic modulus data are available in the Excel file named "*Microrheology Data on MCF-10A, MCF-7, and MDA-MB-231.xlsx*". The data are arranged in chronological order of measurement. This dataset allows the determination of the median viscosity η and elastic modulus G values of as a function of the number of wires treated. This methodology enables us to estimate the minimum amount of wires required to obtain reliable median values. Fig. S7 illustrates that, with about 20 MRS measurements, the median η and G values reach a stationary plateau consistent with results derived from the complete dataset. Beyond 20 processed wires, the median values remain constant, while only the standard error diminishes.

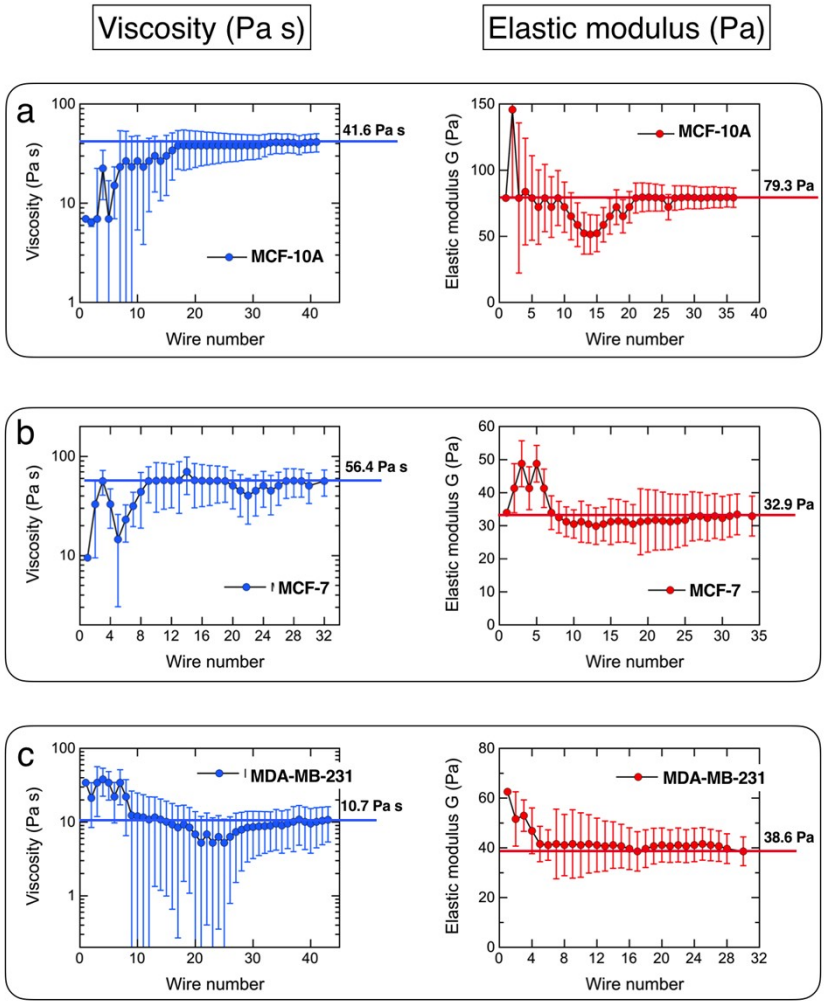

Figure S7 : *Median intracellular viscosity η and elastic modulus G for MCF-10A (a), MCF-7 (b) and MDA-MB-231 (c) as a function of the number of magnetic wires treated.*

Supporting Information S8

Apparent elastic and Young moduli measured according to literature

References	Techniques	Apparent elastic/Young Modulus (Pa)			Elasticity ratio
		MCF-10A	**MCF-7**	**MDA-MB-231**	
Li *et al.* 2008 [12]	AFM	730	410		$E_{MCF\text{-}10A}/E_{MCF\text{-}7}$ = 1.4-1.8
Nikkhah *et al.* 2010 [13]	AFM	1130 ± 840		510 ± 350	$E_{MCF\text{-}10A}/E_{MDA\text{-}MB\text{-}231}$ = 2.2
Agus *et al.* 2013 [14]	AFM	1500		1000	$E_{MCF\text{-}10A}/E_{MDA\text{-}MB\text{-}231}$ = 1.5
Rother *et al.* 2014 [15]	AFM-based microrheology	1370 ± 70		690 ± 60	$E_{MCF\text{-}10A}/E_{MDA\text{-}MB\text{-}231}$ = 2.0
Calzado-Martín *et al.* 2016 [16]	AFM	700 ± 300	500 ± 100	300 ± 100	$E_{MCF\text{-}10A}/E_{MCF\text{-}7}$ = 1.4 $E_{MCF\text{-}10A}/E_{MDA\text{-}MB\text{-}231}$ = 2.33
Mandal et al. 2016 [17]	Optical tweezers-based active microrheology	42.2 ± 3.8		21.4 ± 1.5	$G_{MCF\text{-}10A}/G_{MDA\text{-}MB\text{-}231}$ = 1.97
Nematbakhsh *et al.* 2017 [18]	AFM on adhered or in microwells-confined cells	550	450	200	$E_{MCF\text{-}10A}/E_{MCF\text{-}7}$ = 1.22 $E_{MCF\text{-}10A}/E_{MDA\text{-}MB\text{-}231}$ = 2.75
Hu et *et al.* 2018 [19]	Shear assay and digital imaging correlation	3600 ± 1500		260 ± 150	$E_{MCF\text{-}10A}/E_{MDA\text{-}MB\text{-}231}$ = 14
Dannhauser *et al.* 2020 [20]	Microfluidic chip for cell deformation measurements				$E_{MCF\text{-}10A}/E_{MDA\text{-}MB\text{-}231}$ = 6
This work	**Magnetic wires elasticity cytoplasm**	**79.3 ± 7.3**	**32.9 ± 6.0**	**38.6 ± 5.8**	**$G_{MCF\text{-}10A}/G_{MCF\text{-}7}$ = 2.44** **$G_{MCF\text{-}10A}/G_{MDA\text{-}MB\text{-}231}$ = 2.05**

Table S2: *Literature data on elastic moduli measured on the three cell lines MCF-10A, MCF-7 and MDA-MB-231. E refers to the apparent Young's modulus and G to the instantaneous shear modulus. The last column gives the elasticity ratios for all the results collected, and we can see that, except for the work by Dannhauser et al. [20] and Hu et al. [19], they are of the order of 2 for all the measurements, leading to the conclusion that metastatic cells are softer than normal-like cells [21].*

References

[1] A. Volk, C.J. Kähler, Density model for aqueous glycerol solutions, *Experiments in Fluids*, 59 (**2018**) 75. doi:10.1007/s00348-018-2527-y

[2] B. Frka-Petesic, K. Erglis, J.-F. Berret, A. Cebers, V. Dupuis, J. Fresnais, O. Sandre, R. Perzynski, Dynamics of Paramagnetic Nanostructured Rods under Rotating Field, *J. Magn. Magn. Mater.*, 323 (**2011**) 1309-1313. doi:10.1016/j.jmmm.2010.11.036

[3] F. Loosli, M. Najm, R. Chan, E. Oikonomou, A. Grados, M. Receveur, J.-F. Berret, Wire-Active Microrheology to Differentiate Viscoelastic Liquids from Soft Solids, *ChemPhysChem*, 17 (**2016**) 4134-4143. doi:10.1002/cphc.201601037

[4] J.-F. Berret, G. Porte, J.P. Decruppe, Inhomogeneous shear rows of wormlike micelles: A master dynamic phase diagram, *Phys. Rev. E*, 55 (**1997**) 1668-1676. doi:10.1103/PhysRevE.55.1668

[5] J.-F. Berret, Rheology of wormlike micelles: Equilibrium properties and shear banding transitions, *Mol. Gels*, (**2006**) 667-+. doi:10.1007/1-4020-3689-2_20

[6] J.F. Berret, J. Appell, G. Porte, Linear Rheology of Entangled Wormlike Micelles, *Langmuir*, 9 (**1993**) 2851-2854. doi:10.1021/la00035a021

[7] S. Lerouge, J.-F. Berret, Shear-Induced Transitions and Instabilities in Surfactant Wormlike Micelles, in: K. Dusek, J.F. Joanny (Eds.) Polymer Characterization: Rheology, Laser Interferometry, Electrooptics, Springer-Verlag, Berlin Heidelberg, 2010, pp. 1-71.

[8] J.-F. Berret, Local Viscoelasticity of Living Cells Measured by Rotational Magnetic Spectroscopy, *Nat. Commun.*, 7 (**2016**) 10134. doi:10.1038/ncomms10134

[9] C.L. Bostoen, J.-F. Berret, A Mathematical Finance Approach to the Stochastic and Intermittent Viscosity Fluctuations in Living Cells, *Soft Matter*, 16 (**2020**) 5959-5969. doi:10.1039/C9SM02534K

[10] L.-P.-A. Thai, F. Mousseau, E. Oikonomou, M. Radiom, J.-F. Berret, Effect of Nanoparticles on the Bulk Shear Viscosity of a Lung Surfactant Fluid, *ACS Nano*, 14 (**2020**) 466-475. doi:10.1021/acsnano.9b06293

[11] M.M. Tirado, C.L. Martinez, J.G. Delatorre, Comparison of Theories for the Translational and Rotational Diffusion-Coefficients of Rod-Like Macromolecules - Application to Short DNA Fragments, *J. Chem. Phys.*, 81 (**1984**) 2047-2052. doi:10.1063/1.447827

[12] Q.S. Li, G.Y.H. Lee, C.N. Ong, C.T. Lim, AFM Indentation Study of Breast Cancer Cells, *Biochem. Biophys. Res. Commun.*, 374 (**2008**) 609-613. doi:10.1016/j.bbrc.2008.07.078

[13] M. Nikkhah, J.S. Strobl, R. De Vita, M. Agah, The Cytoskeletal Organization of Breast Carcinoma and Fibroblast Cells inside three Dimensional (3-D) Isotropic Silicon Microstructures, *Biomaterials*, 31 (**2010**) 4552-4561. doi:10.1016/j.biomaterials.2010.02.034

[14] D.B. Agus, J.F. Alexander, W. Arap, S. Ashili, J.E. Aslan, R.H. Austin, V. Backman, K.J. Bethel, R. Bonneau, W.-C. Chen*, et al.*, A Physical Sciences Network Characterization of Non-Tumorigenic and Metastatic Cells, *Sci. Rep.*, 3 (**2013**) 1449. doi:10.1038/srep01449

[15] J. Rother, H. Nöding, I. Mey, A. Janshoff, Atomic Force Microscopy-Based Microrheology Reveals Significant Differences in the Viscoelastic Response between Malign and Benign Cell Lines, *Open Biol.*, 4 (**2014**) 140046. doi:10.1098/rsob.140046

[16] A. Calzado-Martín, M. Encinar, J. Tamayo, M. Calleja, A. San Paulo, Effect of Actin Organization on the Stiffness of Living Breast Cancer Cells Revealed by Peak-Force Modulation Atomic Force Microscopy, *ACS Nano*, 10 (**2016**) 3365-3374. doi:10.1021/acsnano.5b07162

[17] K. Mandal, A. Asnacios, B. Goud, J.-B. Manneville, Mapping Intracellular Mechanics on Micropatterned Substrates, *Proc. Natl. Acad. Sci.*, 113 (**2016**) E7159-E7168. doi:10.1073/pnas.1605112113
[18] Y. Nematbakhsh, K.T. Pang, C.T. Lim, Correlating the Viscoelasticity of Breast Cancer Cells with their Malignancy, *Converg. Sci. Phys. Oncol.*, 3 (**2017**) 034003. doi:10.1088/2057-1739/aa7ffb
[19] J. Hu, Y. Zhou, J.D. Obayemi, J. Du, W.O. Soboyejo, An investigation of the viscoelastic properties and the actin cytoskeletal structure of triple negative breast cancer cells, *J. Mech. Behav. Biomed. Mater.*, 86 (**2018**) 1-13. doi:10.1016/j.jmbbm.2018.05.038
[20] D. Dannhauser, M.I. Maremonti, V. Panzetta, D. Rossi, P.A. Netti, F. Causa, Mechanical phenotyping of breast cell lines by in-flow deformation-dependent dynamics under tuneable compressive forces, *Lab. Chip*, 20 (**2020**) 4611-4622. doi:10.1039/D0LC00911C
[21] C. Alibert, B. Goud, J.-B. Manneville, Are Cancer Cells Really Softer than Normal Cells?, *Biol. Cell*, 109 (**2017**) 167-189. doi:https://doi.org/10.1111/boc.201600078